

Electronic states of semiconductor clusters: Homogeneous and inhomogeneous broadening of the optical spectrum

A. P. Alivisatos, A. L. Harris, N. J. Levinos, M. L. Steigerwald, and L. E. Brus

Citation: *J. Chem. Phys.* **89**, 4001 (1988); doi: 10.1063/1.454833

View online: <http://dx.doi.org/10.1063/1.454833>

View Table of Contents: <http://jcp.aip.org/resource/1/JCPSA6/v89/i7>

Published by the [AIP Publishing LLC](#).

Additional information on *J. Chem. Phys.*

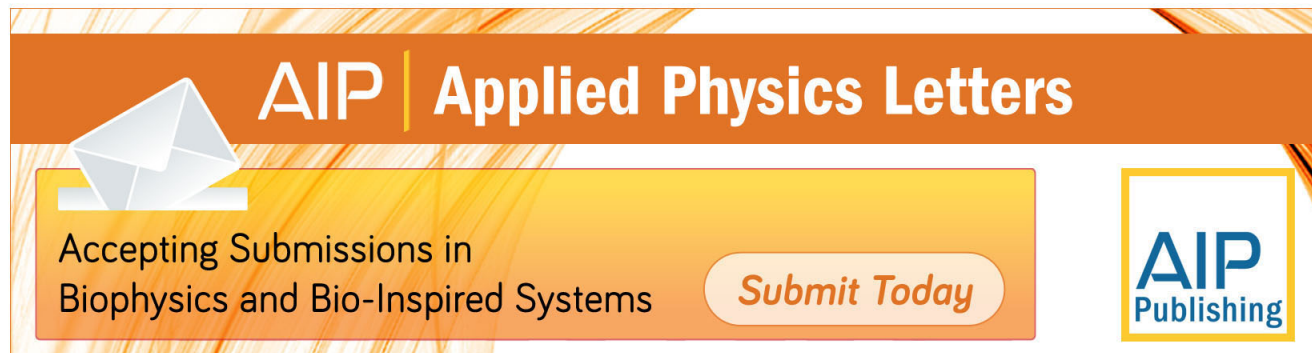
Journal Homepage: <http://jcp.aip.org/>

Journal Information: http://jcp.aip.org/about/about_the_journal

Top downloads: http://jcp.aip.org/features/most_downloaded

Information for Authors: <http://jcp.aip.org/authors>

ADVERTISEMENT



AIP | Applied Physics Letters

Accepting Submissions in
Biophysics and Bio-Inspired Systems

Submit Today

**AIP
Publishing**

Electronic states of semiconductor clusters: Homogeneous and inhomogeneous broadening of the optical spectrum

A. P. Alivisatos,^{a)} A. L. Harris, N. J. Levinos, M. L. Steigerwald, and L. E. Brus
AT&T Bell Laboratories, 600 Mountain Avenue, Murray Hill, New Jersey 07974

(Received 29 March 1988; accepted 24 June 1988)

The homogeneous (single-cluster) and inhomogeneous contributions to the low temperature electronic absorption spectrum of 35–50 Å diameter CdSe clusters are separated using transient photophysical hole burning. The clusters have the cubic bulk crystal structure, but their electronic states are strongly quantum confined. The inhomogeneous broadening of these features arises because the spectrum depends upon cluster size and shape, and the samples contain similar, but not identical, clusters. The homogeneous spectrum, which consists of a peak 140 cm^{-1} (17 meV) wide, with a phonon sideband and continuum absorption to higher energy, is compared to a simple molecular orbital model. Electron–vibration coupling, which is enhanced in small clusters, contributes to the substantial broadening of the homogeneous spectrum. The inhomogeneous width of the lowest allowed optical transition was found to be 940 cm^{-1} , or seven times the homogeneous width, in the most monodisperse sample.

I. INTRODUCTION

Semiconductor clusters with diameters of 20–200 Å, containing a few hundred to tens of thousands of atoms, have been actively investigated in recent years to understand the dependence of their electronic properties on size.¹ These clusters are large enough so that the bulk crystal structure is obtained, but are too small to form continuous bands of electronic states. A major change in the electronic structure occurs when the cluster diameter is comparable to, or smaller than, the diameter of the bulk exciton (typically 20–80 Å for II–VI semiconductors). The finite size of the cluster should transform the continuous bands of the bulk crystal into a series of discrete states, or molecular orbitals, and shift the lowest allowed absorptions to higher energies. The energies and separations of these states, the optical transition probabilities between them and the transition line shapes and linewidths are properties which must be measured and understood before an adequate picture of these clusters can emerge. This picture will contribute to an understanding of the potentially interesting nonlinear optical properties of the clusters as well.²

By preparing various size clusters in liquid solutions and measuring the absorption spectrum, it has been established that the quantum confinement of the electronic states is responsible for an observed shift of the absorption onset to higher energy with decreasing cluster size. The discrete transitions have not been directly studied, however, because of inhomogeneous broadening of the optical transitions arising from the presence of similar, but not identical, clusters in the samples. This is because the electronic properties of the clusters are strongly size dependent and even the best synthetic methods prepare a distribution of sizes.

In this paper, we report measurements of the linear homogeneous absorption spectrum of CdSe clusters, using

transient photophysical hole burning to remove the inhomogeneous broadening. The focus is on features of the spectrum near the absorption onset in clusters of CdSe in the 35–55 Å diameter range. A 45 Å diameter CdSe cluster is about 8 unit cells across, contains approximately 1800 atoms, and is about half the volume of the bulk exciton. Such a cluster shows strong quantum confinement, with the lowest excited state appearing in absorption at 2.3 eV (540 nm), shifted 0.46 eV higher than the absorption edge of bulk CdSe (1.84 eV, 674 nm).

In a simple model of cluster electronic structure,^{1,3} the quantum-confined states for an electron-hole pair in such a cluster can be calculated within the effective mass approximation. Each electronic band of the bulk solid is transformed into a series of discrete well-separated molecular orbitals. The energy levels of the resulting particle-in-a-sphere wavefunctions for a 45 Å diameter CdSe cluster are shown in Fig. 1(a). The states are labeled according to their symmetry. The single conduction band gives rise to one set of unoccupied states, while the spin-orbit split valence band gives rise to two sets of occupied states. The optical spectrum, shown in Fig. 1(b), is predicted to consist of discrete transitions between valence and conduction levels with the same quantum numbers. The lowest is the 1S–1S, or HOMO–LUMO transition, shifted 0.55 eV from the bulk band gap. The second optical transition occurs 0.42 eV higher in energy. This model neglects the Coulomb attraction between the electron and the hole, and therefore overestimates the shift of the HOMO–LUMO to higher energy. This simplification does not, however, change the overall shape of the predicted spectrum.⁴

In Sec. II, properties (other than optical) of the cluster samples are presented, followed by a description of the hole-burning apparatus and procedure. The results of the hole-burning experiments are reported in Sec. III. In Sec. IV, the relationship between the shape of the spectral hole which is burned and the linear homogeneous absorption spectrum is examined. Finally, the consequences of the observed homogeneous absorption spectrum are discussed.

^{a)} Present address: Department of Chemistry, University of California, Berkeley, CA 94720.

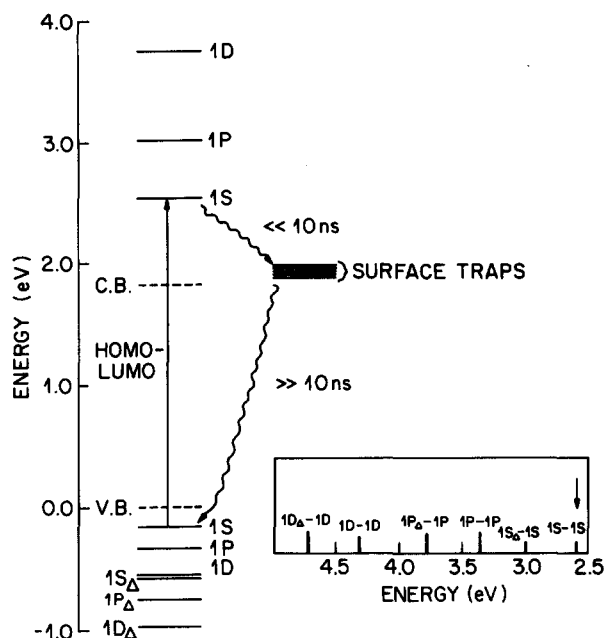


FIG. 1. (a) Energy level diagram for a spherical cluster of CdSe 45 Å in diameter, from elementary theory (Refs. 1 and 3). Dotted lines are bulk band edges. The straight arrow shows the HOMO-LUMO transition. The wiggly arrows indicate the probable nonradiative decay times. Δ labels spin-orbit split-off states. (b) (inset) Stick diagram of the energies at which optical transitions occur within the MO model. The arrow denotes the HOMO-LUMO transition.

II. EXPERIMENTAL

A. CdSe cluster preparation and characterization

The preparation and characterization of the CdSe cluster samples used in these experiments has been described in detail elsewhere.⁵ One special feature of these clusters is that the surface Se atoms have been derivatized with phenyl groups, which prevents aggregation of the clusters, and makes them chemically stable. These surface-derivatized clusters can be isolated as powders and redispersed in a nonpolar solvent without permanent cluster fusion. Following the initial preparation, most of the clusters used in the present experiments were subjected to heat treatments. The clusters were refluxed under inert atmosphere for 1 h at 115 °C in pyridine. One sample was refluxed in quinoline at 238 °C for 30 min. These heat treatments sharpen the room temperature absorption spectrum. Their effect on the homogeneous and inhomogeneous spectra will be discussed further in Sec. III. After refluxing, the clusters were again isolated as a powder and stored in the dark at 0 °C.

These cluster samples have been characterized by transmission electron microscopy, x-ray powder diffraction, small angle x-ray scattering, and HPLC,⁵ as well as by resonance Raman and infrared vibrational spectroscopy,^{5,6} and by NMR.^{5,7} The clusters are crystalline with the cubic, rather than hexagonal, crystal structure. The lattice constant, measured by x-ray diffraction powder patterns is 6.05 Å, in good agreement with the value for bulk cubic CdSe. The mean diameter was measured by TEM and small angle x-ray scattering.

For all of the optical experiments, the CdSe clusters

were homogeneously dispersed in a polystyrene film. 1–5 mg of cluster powder was redissolved in 1 ml pyridine, and to this solution 300 mg of polystyrene beads (Aldrich, Stock No. 18 247-7) were added. Once this mixture was homogeneous, a film was cast from the solution by evaporation of the pyridine. At this concentration, and assuming the clusters are homogeneously dispersed in the film, the mean distance between clusters is about 680 Å, or 15 cluster diameters.

B. Hole-burning apparatus and procedure

For measurements between 7.5 and 200 K the polystyrene films containing the clusters were sandwiched between two 1 mm thick 0° sapphire windows and were mounted in a continuous-flow He cryostat. The temperature was measured with a Si diode attached to one of the sapphire windows. For 1.6 K measurements the films were immersed directly in superfluid helium.

A schematic of the hole-burning apparatus is shown in Fig. 2. Hole-burning spectra were obtained using two 3 ns 10 Hz dye lasers with a 0.4 cm⁻¹ linewidth, pumped by the third harmonic of a Q-switched Nd:YAG laser. The beams from the two dye lasers were telescoped to 3 mm beam diameters and counterpropagated through the sample. The output of one dye laser acted as the optical pump, with an intensity at the sample between 25 and 400 μJ cm⁻². The second dye laser acted as the optical probe with an intensity of 2.5–50 μJ cm⁻². Generally, the probe dye laser was delayed by 5 ns relative to the pump, although the probe delay was varied to investigate the lifetime of the transient bleach induced by the pump laser. The transmission of the probe laser was measured using large area photodiodes (EG&G DT-110) coupled to gated A/D converters and a microcomputer. The change in optical density was computed based on the transmission of the probe laser with and without the pump pulse incident on the sample. About 100–200 pulses were averaged at each wavelength to reduce the noise to several parts in 10⁴. In a typical experiment, the pump laser was maintained at a fixed wavelength in the absorption band of the sample, while the probe laser was tuned. A spectrum of the transient bleach induced by the pump was thereby obtained. Alternatively,

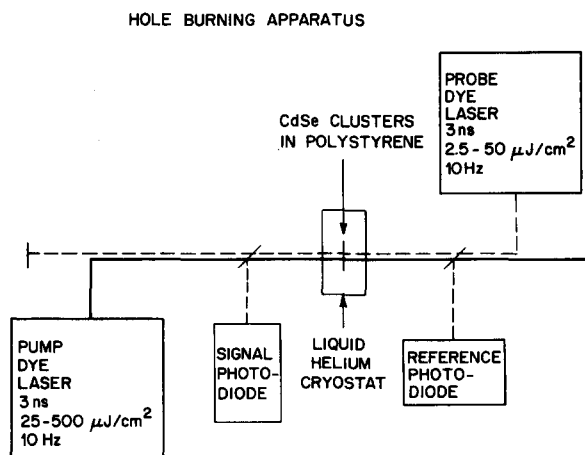


FIG. 2. Schematic of the apparatus used to obtain hole-burning spectra.

the probe was maintained at a fixed wavelength while the pump was scanned, giving somewhat different information.

III. RESULTS

A. Holes can be burned

The electronic absorption spectrum of a 45 Å diameter CdSe cluster sample at 7.5 K in polystyrene is shown in Fig. 3(a). This spectrum shows features which are typical of II–VI cluster samples smaller than the bulk exciton.¹ The spectrum is composed of two parts, a broad shoulder at the absorption onset, merging on the high energy side with a continuously rising absorption. The shoulder has been attributed to the HOMO–LUMO transition, which is shifted by quantum confinement to 2.3 eV from the bulk band gap of 1.84 eV. Discrete optical transitions are not seen. Holes can, however, be burned in the shoulder at the absorption onset, as shown in Fig. 3(a). A pump laser pulse of 200 $\mu\text{J}/\text{cm}^2$ induces a 10% change in absorption at the position of the pump pulse. The difference spectrum, inverted, is shown magnified in Fig. 3(b). The hole which is burned at 7 K is about 240 cm^{-1} (30 meV) wide.

No permanent change in the sample absorption is induced by the pump pulse. The hole or bleach in the absorption is transient, recovering completely in the 100 ms between successive laser shots at all temperatures. Thus, when the probe pulse *precedes* the pump pulse by a few nanoseconds, no hole spectrum is observed. The bleach intensity

reaches a maximum when the probe just follows the pump (peak separation about 5 ns), and thereafter falls off on a time scale of tens of nanoseconds. Since the time delays were introduced in this case by long optical delay lines, no attempt was made to obtain a quantitative estimate of the hole lifetime.

The intensity of the hole which was burned was linear below 200 $\mu\text{J}/\text{cm}^2$, but was sublinear above that, saturating when the absorption change was about 10%. Most of the experiments were carried out in the linear regime, but because the signal-to-noise improved at higher powers, some were carried out in the saturated region. The shape of the hole, however, showed only very weak dependence on the pump laser power within the range of powers employed.

Holes were burned at low temperature (5–10 K) in several samples with cluster diameters in the range 35–55 Å. Within this limited size range, variations in hole width and shape between different samples were at least as large as any systematic change with particle size, so the size dependence of the hole width and shape cannot be determined from the present experiments. All samples refluxed in pyridine at 115 °C generally showed very similar behavior within this size range, however, and the shape of the spectral hole was investigated in several of these samples.

B. The shape of the spectral hole

The dependence of the hole shape and position on pump wavelength near the sample absorption edge was investigated. Figure 4 demonstrates that the shape of the hole is not a strong function of pump wavelength when the pump is near the absorption onset in the sample. The absorption at 7 K of a sample with 38 Å diameter clusters is shown. The absorption edge is shifted to 2.48 eV (500 nm), somewhat higher than that of the 45 Å cluster in Fig. 3(a). The inverted and expanded difference spectra for holes burned at four different pump wavelengths are shown under the absorption spectrum. The holes are similar in shape, but the peak of the spectral hole always coincides with the pump wavelength.

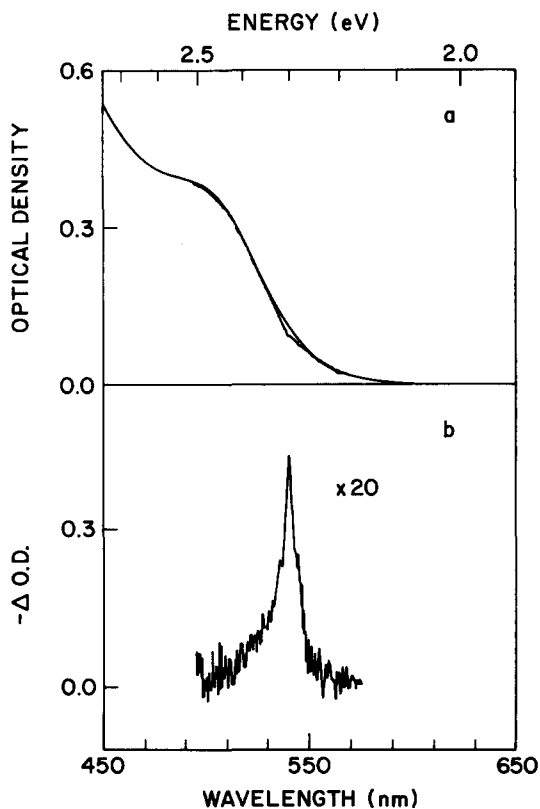


FIG. 3. (a) The electronic absorption spectrum of 45 Å diameter CdSe clusters embedded in polystyrene film at 7 K. Superimposed curve is the transient absorption spectrum after pump excitation (400 $\mu\text{J}/\text{cm}^2$ at 540 nm); (b) the difference spectrum, inverted.

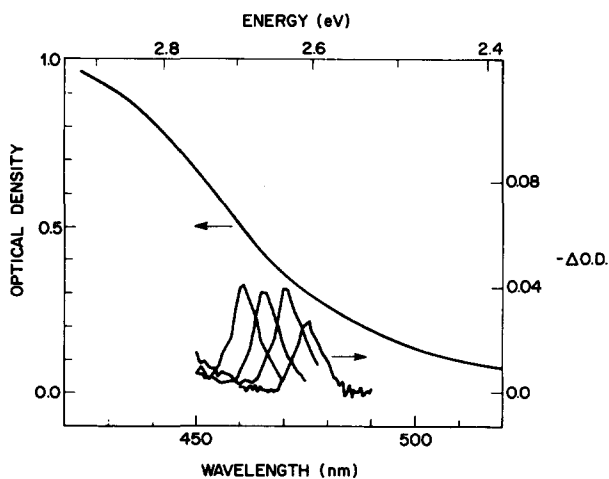


FIG. 4. Upper curve: absorption spectrum of 38 Å CdSe clusters in polystyrene film at 7 K. Lower curves: inverted difference spectra taken after pump excitation at four different pump wavelengths, 460, 465, 470, and 475 nm. A hole always appears centered at the laser pump frequency.

As the pump is tuned to shorter wavelengths, however, the hole shape changes (Fig. 5). When the pump pulse is at the absorption onset [Fig. 5(b), 540 nm], a narrow hole is observed, which is asymmetric, rising more sharply on the low energy side than it falls on the high energy side. When the pump is tuned to a shorter wavelength near the peak of the shoulder [515 nm, Fig. 5(c)], a symmetric peak, riding on a smoothly varying background is obtained. Finally, when the pump pulse is placed on the high energy side of the shoulder [Fig. 5(d), 490 nm], a double peaked hole spectrum is obtained. A narrow peak is observed centered about the laser pump wavelength, while a broader peak is observed at lower energy.

When the pump laser is tuned to an energy significantly higher than the absorption edge of the sample [Fig. 6(a), 440 nm pump], no bleach is seen at the pump wavelength,

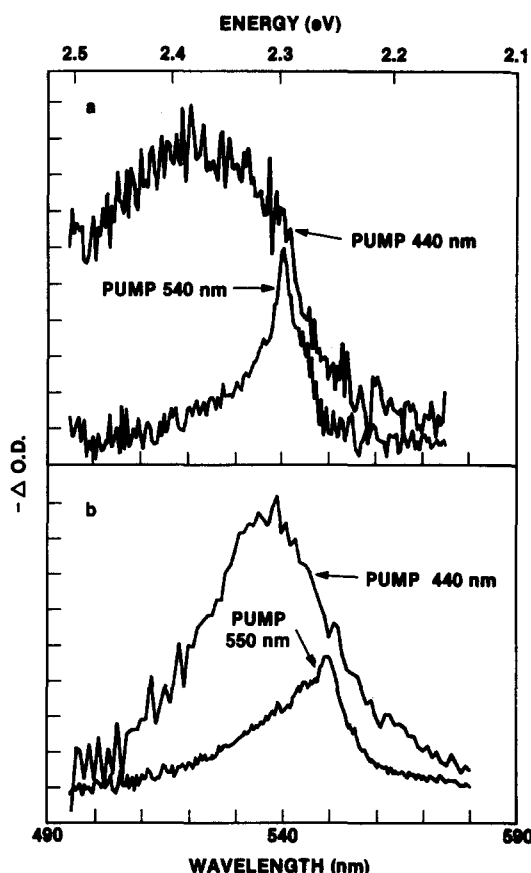


FIG. 6. Transient bleach spectra (inverted and scaled to similar size) observed after 440 and 540 nm pump excitation in 45 Å CdSe clusters at 7 K. (a) Sample refluxed 1 h at 115 °C in pyridine; (b) sample refluxed 1/2 h at 238 °C in quinoline.

but a very broad “hole” appears at the absorption onset. The entire absorption shoulder is partially bleached in this case.

The probe wavelength can also be held fixed near the absorption edge [at the peak of the bleach in Fig. 5(b), for example] while scanning the pump laser wavelength. In this case, the bleach observed by the probe as a function of pump wavelength is shown in Fig. 7, and compared with the spec-

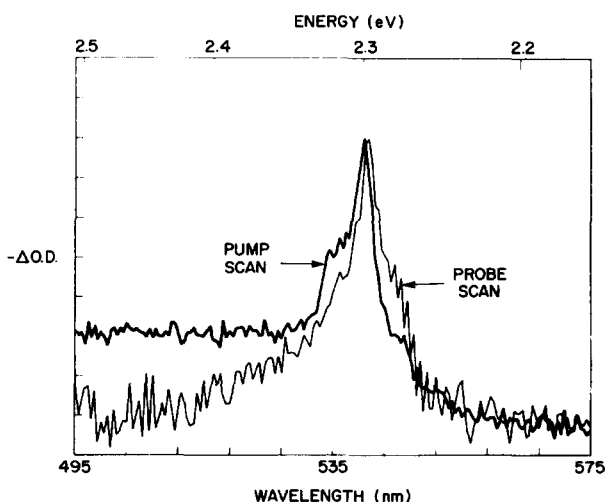


FIG. 7. Transient bleach signals (inverted) observed in two ways. Probe scan as in previous figures, with pump fixed at 540 nm. Pump scan obtained with probe fixed at 540 nm, and pump scanned in wavelength. In both cases, signal is obtained from probe transmission changes.

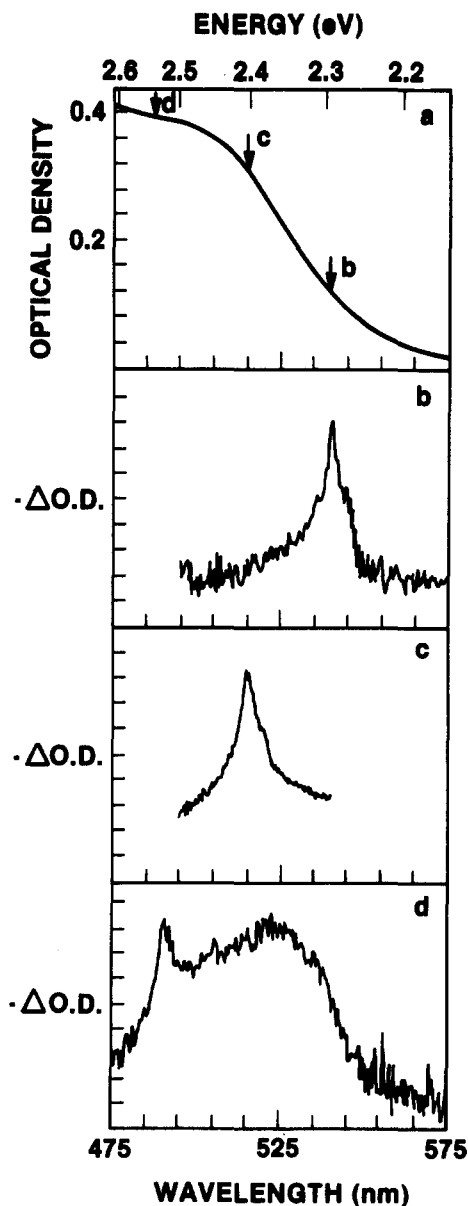


FIG. 5. Transient bleach spectra (inverted) observed after pump excitation at three wavelengths in 45 Å clusters of CdSe at 7 K. (a) Sample absorption spectrum; (b), (c), (d) pump wavelengths as labeled.

trum obtained in the case of a fixed pump with a scanned probe. The pump scan shows a peak, followed by a flat absorption probability at all higher energies. The bleach strength at the fixed probe wavelength was constant for pump wavelengths scanned down to 410 nm, and no evidence of discrete transitions was found in this region. This contrasts with the probe scan, which shows little bleach for probe wavelengths below 500 nm.

C. Temperature dependence of hole linewidth

The temperature dependence of the spectral hole width burned in the spectrum of a 45 Å diameter CdSe sample at 515 nm [Fig. 5(c)] was investigated for temperatures between 1.6 and 200 K. The shape of the hole is a symmetric peak riding on a broad, smoothly varying, temperature insensitive background. The width of the central peak was characterized by fitting a smooth curve to the background and using the fitted curve to subtract the background. The full width at half-maximum of the remaining peak was used to characterize the peak width. The results are shown in Fig. 8. The 240 cm^{-1} zero temperature linewidth is the same in all samples which have been refluxed in pyridine. The peak width increases with temperature above 10 K, and broadens enough by 200 K so that it cannot be unambiguously separated from the background.

D. The effect of heat treatments

The width and to some extent the shape of the holes which are burned depends on sample preparation, and this is illustrated for 45 Å diameter CdSe clusters in Fig. 6. Figure 6(a) shows the results obtained for samples which have been refluxed at 115 °C in pyridine, while Fig. 6(b) shows the results for a sample refluxed in quinoline at 238 °C. It is very difficult to burn a hole in a sample which has received no heat treatment.

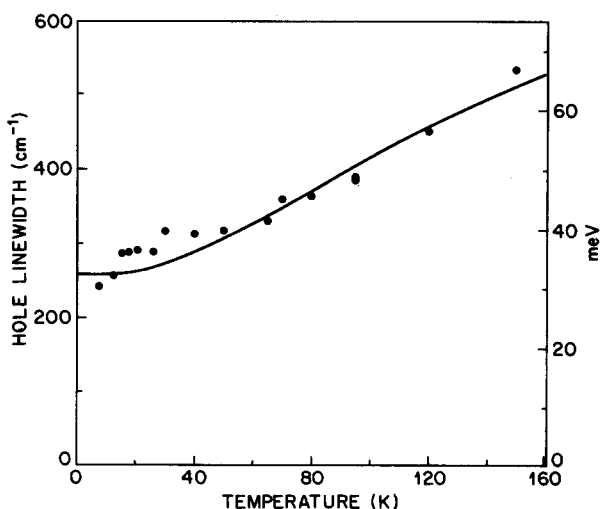


FIG. 8. Temperature dependence of linewidth (FWHM) of HOMO-LUMO transition peak. Solid lines from displaced harmonic oscillator model, which is described in Appendix A.

IV. DISCUSSION

The transient hole-burning experiments demonstrate that the low temperature absorption spectrum of presently available semiconductor cluster samples is dominated by inhomogeneous broadening. In Sec. IV A we obtain an approximate spectrum of a homogeneous subset of clusters, based upon the hole-burning experiments. We also determine the width of the inhomogeneous distribution. In Sec. IV B, this inhomogeneous distribution is discussed. Section IV C is concerned with the physical interpretation of the shape of the homogeneous absorption spectrum.

A. Modeling of the hole-burning experiments

To model the experiments, the homogeneous ground state absorption spectrum $\sigma(\nu)$ is assumed to consist of two parts (see Fig. 9). The first part is the HOMO-LUMO absorption $\sigma_{HL}(\nu)$ consisting of a sharp Gaussian peak and a broader Gaussian sideband. The second part is a continuously rising absorption, $\sigma_c(\nu)$, due to transitions from occupied states below the HOMO to unoccupied states above the LUMO. The widths and relative heights of the features are adjusted to approximately reproduce the bleach feature. The homogeneous (single cluster) spectrum $\sigma(\nu)$ is the sum of these two components.

We assume that upon excitation into *any* level of the cluster, rapid relaxation of the electron and the hole occurs, so that *only* the HOMO-LUMO transition bleaches, while higher energy absorptions are unchanged. The absorption spectrum of an electronically excited cluster which has relaxed to the lowest electronic excited state is then $\sigma_e(\nu)$. We

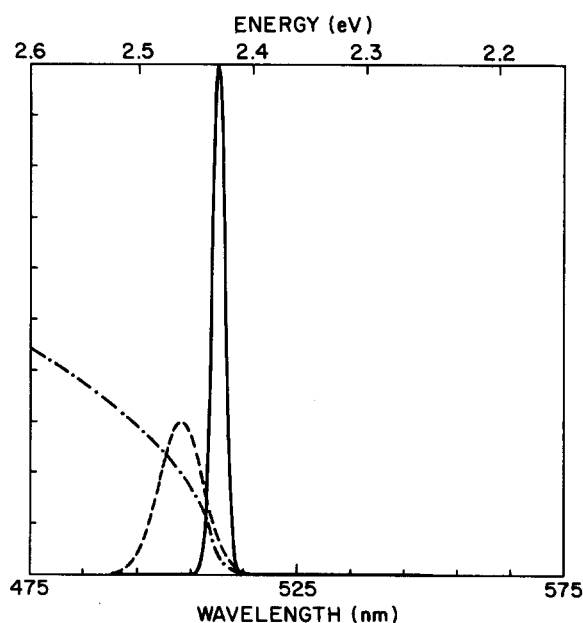


FIG. 9. Components of the model homogeneous cluster absorption spectrum. The solid line is a Gaussian with 1.75 nm width, representing the HOMO-LUMO zero-phonon line; the dashed line is a second Gaussian, representing the HOMO-LUMO phonon sideband with a width of 6 nm and offset 5 nm to higher energy; the dashed-dotted line represents continuum absorption due to all cluster transitions except the HOMO-LUMO, and follows a square root dependence on energy.

note that no fluorescence is observed from the HOMO–LUMO transition itself. Red-shifted fluorescence emission is observed from localized trap states on a microsecond time scale.⁸ Rapid relaxation of the HOMO–LUMO into the trap states must occur after absorption. The subsequent trap relaxation time will determine the recovery of absorption from the ground state.

All the ground state clusters are assumed to have identical homogeneous spectra, inhomogeneously shifted to higher or lower frequencies. This will certainly be the case for inhomogeneity due to variation in cluster size, and polymer film environment. It may not be the case for clusters with different shapes, because departure from spherical geometry could remove degeneracies, but we will assume this effect is not large. Each cluster is labeled according to the position of the center frequency of its HOMO–LUMO peak ν_0 and we reference individual cluster spectra to ν_0 ; the spectrum of a cluster with HOMO–LUMO peak at ν_0 is then $\sigma(\nu - \nu_0)$. The total sample absorption spectrum $\alpha(\nu)$ is obtained by convoluting the homogeneous spectrum $\sigma(\nu - \nu_0)$ with the inhomogeneous distribution $p(\nu_0)$:

$$\alpha(\nu) = NL \int_{-\infty}^{\infty} p(\nu_0) \sigma(\nu - \nu_0) d\nu_0, \quad (1)$$

where N is the total number density of particles, L is the sample thickness, $\sigma(\nu - \nu_0)$ is the absorption cross section at frequency ν of the clusters with HOMO–LUMO peak at ν_0 and the distribution $p(\nu_0)$ is normalized:

$$\int_{-\infty}^{\infty} p(\nu_0) d\nu = 1. \quad (2)$$

Excitation of the sample with a pump of frequency ν_p leads to a change in optical absorption. The change in absorption at frequency ν due to excitation of clusters with HOMO–LUMO frequency ν_0 is

$$\begin{aligned} \Delta\alpha_{\nu_0}(\nu) &= \bar{\Phi}_p \sigma(\nu_p - \nu_0) [\sigma_e(\nu - \nu_0) - \sigma(\nu - \nu_0)] \\ &= -\bar{\Phi}_p \sigma(\nu_p - \nu_0) \sigma_{HL}(\nu - \nu_0), \end{aligned} \quad (3)$$

where $\bar{\Phi}_p$ is the spatial average (through the thickness of the sample) of the pump photon fluence (cm^{-2}):

$$\bar{\Phi}_p = \Phi_p^0 \frac{1 - e^{-\alpha(\nu_p)}}{\alpha(\nu_p)} \quad (4)$$

and where Φ_p^0 is the incident photon fluence. Equation (3) assumes that sample saturation is small, that the sample relaxes to the HOMO–LUMO before being probed, and that relaxation to the ground state to fill the hole can be neglected on the probe time scale. The actual change in absorption of the sample at probe frequency ν is an average of Eq. (3) over the inhomogeneous distribution $p(\nu_0)$:

$$\Delta\alpha(\nu) = \int_{-\infty}^{\infty} p(\nu_0) \Delta\alpha_{\nu_0}(\nu) d\nu_0. \quad (5)$$

Using Eqs. (1) through (5) and the individual components of the cluster spectrum in Fig. 9, the experimental results, and in particular, the changes in the shape of the spectral hole with pump wavelength, are reproduced. Figure 10(a) shows the calculated sample absorption spectrum when an inhomogeneous width of 40 nm FWHM is assumed, and the single particle absorption spectrum from

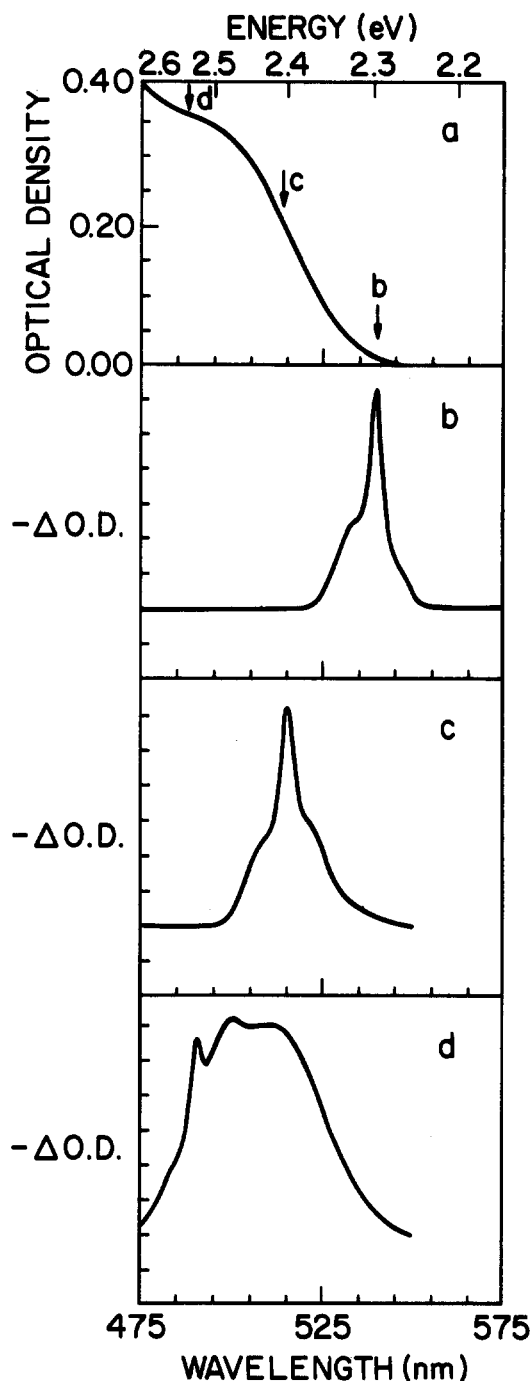


FIG. 10. (a) Calculated total cluster absorption spectrum, assuming the homogeneous spectrum shown in Fig. 9, and a Gaussian inhomogeneous distribution with 40 nm FWHM; (b), (c), (d) calculated transient bleach signals, inverted, for probe scans with the pump placed at the indicated wavelengths. Compare to Fig. 6.

Fig. 9 is used. The simulated bleach spectra obtained for fixed pump frequencies at three points in the inhomogeneous distribution are shown in Figs. 10(b), 10(c), and 10(d), and are comparable to the experimental results in Figs. 5(b), 5(c), and 5(d). The high frequency wing on the hole bleached at 540 nm is reproduced. The double peaked structure of the bleach from a 495 nm pump is also reproduced. It is due to direct excitation of clusters whose HOMO–LUMO transition coincides with the laser frequency (narrow peak at the pump wavelength) and excitation into the higher ener-

gy transitions of all clusters whose HOMO–LUMO transition is lower in energy than the 495 nm pump (broad peak). The simulation can also reproduce the differences seen between the pump scan and the probe scan (experiment, Fig. 7; simulation, Fig. 11).

The shape of the hole which is burned at the sample absorption edge is essentially an autocorrelation of the HOMO–LUMO line shape, weighted by the inhomogeneous distribution [Eq. (5)]. For this reason the spectral hole is broader than the actual homogeneous linewidth. A symmetric Lorentzian line, e.g., is broadened by a factor of 2 in the hole-burning experiment when the inhomogeneous distribution is much broader than the homogeneous linewidth, while a Gaussian line is broadened somewhat less. The spectral bleach is thus about 1.5 to 2 times broader than the width of the actual HOMO–LUMO absorption peak. The widths plotted in Fig. 8 are thus 1.5–2 times the absorption widths. The low temperature spectral hole linewidth of 240 cm^{-1} thus corresponds to a 140 cm^{-1} HOMO–LUMO linewidth.

A much smaller additional broadening of the observed spectral hole can arise if the power of the pump pulse is high enough to excite a large fraction of the clusters whose HOMO–LUMO peak is coincident with the laser frequency. The broadening arises through absorption into the tails of the HOMO–LUMO transitions of nonresonant clusters. The effect is small, so that at the highest power employed in our experiments, a 10% increase in the observed width can be expected.

B. The inhomogeneous distribution

How close to monodisperse is the size distribution in presently available cluster samples? For many experiments,

the distribution can be considered monodisperse when the inhomogeneous width arising from the variation in HOMO–LUMO transition frequency with cluster size and shape is smaller than the 140 cm^{-1} homogeneous width. Assuming that the inhomogeneous width is due entirely to variation in cluster size, we estimate the number of atoms within the CdSe clusters must be 1800 ± 50 in order to fulfill this criterion.

In the present study, we have measured the width of the inhomogeneous distribution of HOMO–LUMO transition frequencies. By pumping at a short enough wavelength, as in Fig. 5(a), 440 nm pump, the pump does not directly excite the HOMO–LUMO transition in any cluster. Instead, all of the clusters are excited approximately equally into their continuous absorption region, regardless of size or shape. Each cluster then relaxes to its lowest electronic excited state on a time scale short compared to the 3 ns pulse widths in the experiment. The HOMO–LUMO transition in each particle is bleached, and the resulting broad bleach is the sum of HOMO–LUMO transitions occurring across the entire inhomogeneous distribution. The narrowest inhomogeneous bleach width we obtained by this method was 940 cm^{-1} at 7 K, or about seven times broader than the low temperature homogeneous width (see Fig. 5). The full width at half maximum of the inhomogeneous distribution is then estimated to be 5 Å, between 46 and 51 Å, corresponding to 28% variation in the number of atoms in the clusters (± 250 atoms). It should be emphasized that the homogeneous width is strongly temperature dependent, and at room temperature the homogeneous and inhomogeneous widths are nearly comparable in the samples used in this study. We note that the broad bleach induced by a pump far above the absorption onset has been observed previously in semiconductor clusters in liquid solution at room temperature,⁹ but no previous hole-burning experiments have been carried out.

The hole-burning experiment is well suited for distinguishing the effect of a preparative method on the intrinsic absorption spectrum from its effect on the distribution of cluster sizes and shapes, and therefore can be an aid in developing better procedures for cluster preparation. For instance, hole burning demonstrates that refluxing in pyridine narrows *both* the inhomogeneous distribution width and the linewidth of a single subset of clusters. On the other hand, the higher temperature treatment in quinoline further narrowed the inhomogeneous width, and changed the homogeneous line shape without further narrowing of the homogeneous linewidth. These heat treatments probably affect the crystalline order, surface structure and shape of the clusters. The polymer film is identical in all of these preparations, bolstering the assumption that it is variation in the clusters and not variation in the cluster environment which provides the main source of inhomogeneous broadening. Presently it is not known whether the relatively broad 17 meV homogeneous width observed in the pyridine and quinoline refluxed samples is intrinsic to clusters of this size, or if further improvements in cluster preparation will lead to narrower linewidths. Nonetheless, broader linewidths are *naturally* to be expected in clusters, compared to bulk exciton linewidths (1 meV for CdSe), for reasons which are presented below.

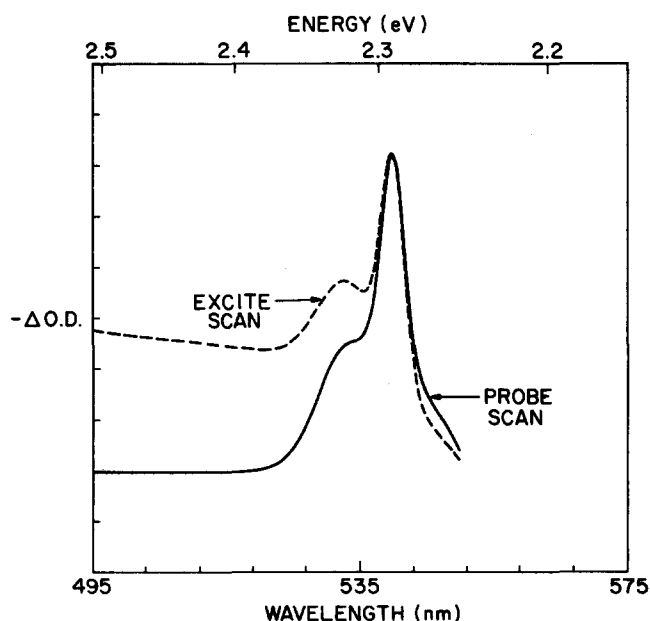


FIG. 11. Solid line, model probe scan with pump at 540 nm. Dashed line, model pump scan with probe at 540 nm. All parameters are the same as in Fig. 10.

C. Interpretation of the homogeneous absorption spectrum

The determination of the homogeneous absorption spectrum of 45 Å diameter CdSe clusters presented above permits a more detailed discussion of cluster electronic structure. There are two noteworthy features of the observed spectrum. The first is the continuum absorption observed at energies just higher than the HOMO–LUMO transition. The MO model predicts a single line in this range. The second feature of interest is the shape of the HOMO–LUMO transition. The molecular orbital model predicts a stick spectrum, but the shape of the actual spectrum is determined by the coupling to vibrations and lifetime broadening.

1. Continuum absorption above the HOMO–LUMO

In the MO model, the HOMO–LUMO transition is followed by another discrete transition, 0.42 eV higher in energy, between the $1S_{\Delta}$ occupied MO to the LUMO (Fig. 1). Optically stronger $1P-1P$, $1D-1D$, etc., MO transitions occur even higher in energy. Several effects may contribute to the continuum absorption which is observed for 1–2 eV just above the HOMO–LUMO transition in the hole-burning experiment. The simple MO model underestimates the number of electronic states in the cluster, and these extra states could contribute to the continuum absorption. For instance, states associated with the surface atoms are ignored, even though they are numerous. In addition, the apparently continuous absorption above the HOMO–LUMO may result from broadening of the higher-lying transitions which appear in the simple MO model, due to fast radiationless relaxation. This would occur if there were strong coupling between higher excited electronic states of the clusters and excited vibrational levels of the HOMO–LUMO state.

2. Shape of the HOMO–LUMO transition: Coupling to vibrations

The HOMO–LUMO transition has the shape shown in Fig. 9, consisting of a narrow peak with a width of about 17 meV, and a wing which is probably an optical phonon sideband. The linewidth of the narrow peak is considerably larger than exciton linewidths in high quality II–VI bulk materials.¹⁰ The linewidth of the HOMO–LUMO transition, if interpreted as an inverse lifetime, represents a lifetime of less than 100 fs. This is consistent with the lack of fluorescence from the HOMO–LUMO transition, in spite of the relatively short (estimated at ~ 10 –100 ns) HOMO–LUMO radiative lifetime. Rapid (< 1 ps) trapping, perhaps to surface defects, may therefore contribute to the low temperature linewidth.

Lifetime broadening does not account, however, for the phonon sideband itself, or for the strong temperature dependence of the width of the narrow HOMO–LUMO peak. Electron–vibration coupling therefore clearly plays an important role in determining the spectral features. We will discuss these effects in this section. Schmitt-Rink, Miller, and Chemla have recently discussed electron–vibration coupling mechanisms in such clusters, considering the electronic states within the same simple molecular orbital pic-

ture.² Their conclusion, that in semiconductor clusters coupling between the electronic and vibrational states is greater than in the bulk, and that the coupling is greatest to acoustic rather than optical vibrations, is in substantial agreement with our results.

Upon excitation of an electron–hole pair, the structure of the lattice changes.¹¹ This structural change is distributed over many vibrational modes in the bulk, but only over a few in the cluster. The coupling to any single vibration is therefore stronger in the cluster. This results in a molecular picture of the coupling; it broadens the absorption features because the ground and excited electronic potential surfaces are shifted in the vibrational coordinate. The Franck–Condon envelope is thereby shifted and broadened; several vibronic transitions may be observed in each vibrational coordinate. If the vibronic transitions are not resolved, they will merge into a broad absorption feature with the width of the Franck–Condon envelope.

The vibrations in the clusters should be determined by elastic constants and vibrational force constants which are similar to those of the bulk semiconductor, because the bonding geometry and bond length are nearly identical to bulk cubic CdSe. We can therefore consider the vibrational modes of the cluster to be analogous to the optical and acoustic modes of the bulk crystal. The electron–vibration coupling mechanisms will also be similar to those acting in the bulk, but modified by the electronic and vibrational localization. Within this picture, therefore, we interpret the wing in the HOMO–LUMO absorption to be due to an LO phonon wing (Franck–Condon envelope), and the sharp peak to be the zero LO phonon peak. The peak itself is broadened by unresolved acoustic phonon replicas (and by lifetime broadening).

The optical modes have a weak dispersion and should have frequencies in the clusters which are near the bulk values. The frequency of these modes has in fact been confirmed by resonance Raman spectroscopy,⁶ with a vibrational line at 205 cm^{-1} , in comparison with a bulk value of 210 cm^{-1} .¹² The exciton in bulk CdSe is coupled by polar interactions to such long wavelength longitudinal optical phonons (Frohlich interaction). This effect arises because when the partially ionic Cd and Se nuclei vibrate, electric fields are created inside the cluster, Coulombically altering the energy of the electron and the hole. How will this coupling change in clusters? $1S$ electron and hole wave functions would have perfect overlap, zero net charge, and thus zero polar coupling. A quantitative estimate of the actual coupling depends upon the correlation between the electron and the hole, and the reduction in the density of states of the vibrational modes. It is therefore beyond the simple MO model used here. Experimentally, the peak of the phonon wing (Fig. 9) is shifted about 35 meV (240 cm^{-1}) from the zero phonon peak, and this provides the estimate that the peak of the Franck–Condon envelope is shifted by about one quantum in the LO mode.

The temperature dependence of the HOMO–LUMO peak itself, shown in Fig. 8, is strong even at low temperature, implying a coupling to low frequency modes. What is the nature of these modes and their coupling to the electronic

transition? To quantify the coupling strength, we can assume that the entire linewidth and its temperature dependence are caused by coupling to a single low frequency mode. A shifted harmonic oscillator model is fit to the data in Fig. 8. The parameters in this model are the mode frequency and a normalized shift X which represents the shift between the ground and excited electronic states, in the coordinate Q of the mode

$$X = \frac{k}{2\hbar\omega}(Q_a - Q_b)^2. \quad (6)$$

Q_a and Q_b are the equilibrium positions of the ground and excited vibrational harmonic potentials, k is the vibrational force constant, and ω is the vibrational frequency, both assumed to be the same in the ground and excited electronic level. The linewidth (FWHM) is calculated from the Franck–Condon envelope for transitions between the vibrational levels of the shifted potentials. The model is described in Appendix A. The calculated linewidth is shown as the solid line in Fig. 8. This fit was obtained with a mode frequency of 47 cm^{-1} and a normalized shift of 1.3 (a shift which is about the width of the vibrational zero point motion).

How does this shift compare to the coupling strength which is expected between the localized electronic states and the acoustic modes of the crystallite? In bulk CdSe, transverse acoustic phonon modes couple to excitons via the piezoelectric interaction, a polar coupling similar to the Frohlich interaction. As is the case for coupling to the LO mode, the strength of this coupling will go to zero in the limit of a very small cluster, but is probably still strong in a cluster of the size considered here. Longitudinal acoustic phonons couple to excitons in the bulk through the deformation potential: compression and expansion of the material, arising from the phonon motion, modulates the Cd–Se bond length, which changes the band gap, and therefore the exciton energy. In contrast to the polar coupling with TA and LO modes, the deformation coupling does not become zero in the limit of strong electronic confinement. The coupling strength will therefore *increase* in smaller clusters due to localization of the vibrational motion. In addition, the strength of the deformation interaction can be estimated directly using the simple 1S particle-in-a-sphere wave functions: the electron–hole Coulomb interaction is only a perturbation on the interaction strength in this case.

To estimate the coupling strength to longitudinal acoustic modes, we assume that the acoustic mode dispersion curves in the clusters are similar to those in the bulk. The modes are, however, discrete; if we approximate the longitudinal acoustic dispersion curve as linear with a slope given by the speed of sound, the allowed mode periods would be integral multiples of the round trip time in the cluster. An estimate of the coupling is made in Appendix B, treating the confined longitudinal acoustic modes as radial compression modes of an elastic sphere. All of the parameters in the calculation are available from measurements in bulk CdSe. The first radial mode in a 45 Å sphere of CdSe is estimated to have a frequency of 27 cm^{-1} . The estimated 1S–1S normalized shift X in the coordinate of the first radial mode of the

sphere, is 0.17. This estimate can be compared to the single oscillator model, which fit the experimental data with a normalized shift of 1.3 and a mode frequency of 47 cm^{-1} . Physically, a normalized shift of 1 in the $n = 1$ mode corresponds to a dilation of the cluster of several parts in 10^4 upon electronic excitation. Although there is not quantitative agreement, the results from these very simple single mode models suggest that such coupling can account for the order of magnitude of the HOMO–LUMO broadening. Note that the calculated broadening does not include broadening arising from coupling to transverse acoustic modes or to the surrounding medium (e. g., polymer matrix).

The deformation potential model sets a lower limit to the optical linewidths in such crystallites which is much greater than the linewidths in similar bulk materials. In fact, for a fixed vibrational frequency, the coupling scales as the inverse volume of the crystallite [Eq. (5), Appendix B]. The coupling to individual modes in the bulk is much weaker, although the density of vibrational states is much higher. The difference between the bulk and the crystallite is that although many small couplings in the bulk creates a phonon wing, the zero phonon line is retained. In the crystallite, strong coupling to a few modes broadens the Franck–Condon envelope, and the zero phonon line is lost. At the opposite limit, molecular spectra in low temperature matrices sometimes show resolved vibronic transitions which are very narrow, although not always.¹³ For very small crystallites with a lower density of vibrational levels (and perhaps with fewer relaxation pathways, so that the vibronic transitions are narrow), the vibronic transitions should be resolved, and narrow resonances may be regained.

V. CONCLUSIONS AND SUMMARY

Transient photophysical hole burning separates the homogeneous and inhomogeneous contributions to the width of the absorption spectrum in samples of 35 to 50 Å diameter CdSe clusters. The sample spectrum at low temperature is dominated by inhomogeneous broadening, which is probably due to a distribution of cluster sizes. The homogeneous line is strongly temperature dependent, so that at room temperature it is within a factor of 2 of the total linewidth. The inhomogeneous distribution can be narrowed by refluxing at 115°C in pyridine, and this also narrows the homogeneous linewidth, suggesting that the initial annealing process contributes to better crystallinity and surface ordering in the clusters. Refluxing at higher temperatures in quinoline further narrows the inhomogeneous distribution, but does not improve the homogeneous line. This indicates that the homogeneous linewidths observed may have reached limits imposed by broadening mechanisms intrinsic to small clusters.

The experiments are all consistent with a homogeneous cluster absorption spectrum which consists of a HOMO–LUMO peak and vibrational sideband followed by continuous absorption to higher energies. The HOMO–LUMO vibrational sideband is assigned to coupling to the longest wavelength LO vibration of the cluster, at 207 cm^{-1} by the Frohlich interaction. The linewidth of the HOMO–LUMO peak itself is approximately 17 meV (140 cm^{-1}) at 1.5 – 7 K ,

and increases approximately linearly with temperature. The broadening appears to be dominated by strong coupling to acoustic vibrations in the cluster. In particular, deformation potential coupling to the localized longitudinal acoustic modes is strong. Trapping to surface states may also contribute to the linewidth by lifetime broadening.

Unlike the HOMO–LUMO absorption, the higher-lying continuous absorption is not consistent with the elementary MO model which predicts discrete transitions. It is likely that the higher-lying discrete states are broadened by rapid relaxation (subpicosecond time scale) into the HOMO–LUMO level.

This study provides the first clear picture of the extent to which relatively strongly quantum-confined semiconductor clusters show a new discrete spectrum of electronic states, and the coupling mechanisms which broaden those states. Further studies as a function of size and surface arrangement, in CdSe and in other semiconductor materials are very desirable.

ACKNOWLEDGMENTS

The authors gratefully acknowledge discussions with S. Schmitt-Rink, D. A. B. Miller, D. S. Chemla, M. G. Bawendi, T. D. Harris, and D. J. Doren.

APPENDIX A: SHIFTED HARMONIC OSCILLATORS

A shifted harmonic oscillator model is used to estimate coupling which can account for the temperature dependence of the HOMO–LUMO linewidth. The electronic state is assumed to couple to one vibrational coordinate only. The absorption linewidth at low temperature is determined by the Franck–Condon envelope for transitions from the ground vibrational level of the ground electronic level. The temperature dependence of the line is determined by thermal population of vibrational levels of the ground state, which affects the thermally averaged Franck–Condon envelope. The Franck–Condon factor for the transition from mode m in the ground electronic state to mode n in the excited electronic state is given for shifted harmonic oscillators by¹⁴

$$|\langle m|n \rangle|^2 = e^{-X} \left(\frac{n!}{m!} \right) X^{m-n} [L_n^{m-n}(X)]^2. \quad (\text{A1})$$

X is the normalized shift of the harmonic oscillator curves, as defined in the text [Eq. (6)]. $L_n^{m-n}(X)$ is the associated Bessel function.

To apply this model to the experimental data, a vibrational frequency was assumed, and the normalized shift X was set so that the width of the Franck–Condon envelope matched the 140 cm^{-1} width of the low temperature cluster HOMO–LUMO transition. The temperature dependence of the linewidth was then calculated, based upon the population of the excited vibrational levels of the electronic ground state, and the Franck–Condon factors from those excited vibrational levels. The solid line in Fig. 8 illustrates the best fit, which was obtained for a vibrational frequency of 47 cm^{-1} . The normalized shift in the vibrational coordinate upon electronic excitation is 1.3, or about the width of the zero point motion in the vibrational coordinate.

APPENDIX B: DEFORMATION POTENTIAL COUPLING AND LINEWIDTH

The local change in energy due to the vibrational motion is related to the static deformation shifts of the band edges in the bulk semiconductor by the Bardeen–Shockley relation for the coupling Hamiltonian H_{dc} ¹⁵:

$$H_{dc} = D_e \Delta(r_e) - D_h \Delta(r_h), \quad (\text{B1})$$

where D_e and D_h are deformation potentials of the conduction (electron) and valence (hole) bands and $\Delta(r)$ is the local dilation of the lattice resulting from vibrational motion. The total coupling energy E_{dc} in first order perturbation is the average of H_{dc} over the $1S$ electronic wave functions of the sphere

$$E_{dc} = \int \Psi_0(\mathbf{r}_e, \mathbf{r}_h) H_{dc} \Psi_0(\mathbf{r}_e, \mathbf{r}_h) d^3\mathbf{r}_e d^3\mathbf{r}_h, \quad (\text{B2})$$

$$\Psi_0(\mathbf{r}_e, \mathbf{r}_h) = \psi_0(\mathbf{r}_e) \psi_0(\mathbf{r}_h).$$

The $1S$ wave functions are radially symmetric, and may be written

$$\psi_0(r) = \frac{1}{(2\pi R)^{1/2}} \sin\left[\frac{\pi r}{R}\right], \quad (\text{B3})$$

where R is the radius of the crystallite.

The electron and hole coordinates are not coupled, so the integral (B2) separates:

$$E_{dc} = (D_e - D_h) 4\pi \int_0^R dr r^2 [\psi(r)]^2 \Delta(r). \quad (\text{B4})$$

We estimate E_{dc} as follows. The vibrational modes are taken to be those of an isotropic elastic sphere. The elastic constants are assumed to be the same as bulk CdSe. The modes which are coupled most strongly by the deformation potential are the radial compression modes of the sphere. The dilation in the radial modes, given by Love¹⁶ is

$$\Delta(r) = \frac{\delta_n \sin(h_n r)}{h_n r} Q_n, \quad (\text{B5})$$

where δ_n is the maximum dilation at the sphere center and Q_n is a unitless vibrational normal coordinate, in the n th radial mode. The frequency of the n th vibrational mode is given by

$$\omega_n = h_n \left(\frac{C_{11}}{\rho} \right)^{1/2}.$$

h_n is found from the solution of

$$\frac{\tan(h_n r)}{h_n r} = \frac{1}{1 - (C_{44}/4C_{11}) h_n^2 R^2}, \quad (\text{B6})$$

where C_{11} and C_{44} are the elastic constants of the sphere. C_{11}/C_{44} in CdSe is about 5,¹² so the solutions of Eq. (B6) are very nearly given by $h_n = n\pi/R$, where $n = 1, 2, 3, \dots$. The deformation coupling energy E_{dc} is therefore approximately given from Eqs. (B5) and (B6) by

$$E_{dc} = Q_n \frac{2\delta_n (D_e - D_h)}{\pi} \int_0^R \sin \frac{n\pi r}{R} dr = Q_n d, \quad (\text{B7})$$

where d is the coupling parameter for the n th mode. The value of the integral in Eq. (B7) is 0.97 for the $n = 1$ mode, and drops off rapidly for higher modes.

For the $n = 1$ mode we can estimate the coupling energy, which is linear in the normal coordinate (let $Q = Q_1$). This energy adds to the quadratic potential energy of the vibrational potential energy in the excited electronic state. This shifts the equilibrium positions of the potential energy curves in the ground (Q_a) and excited (Q_b) electronic states. E_b is the potential energy for vibrational motion in the excited electronic state and E_a is the potential energy for the ground electronic state:

$$E_b = E_a + E_{dc} = \frac{1}{2}k(Q - Q_a)^2 + Qd \\ = \frac{1}{2}k(Q - Q_b)^2.$$

Therefore, $Q_b = -d/k$. The normalized shift of the excited state vibrational coordinate, from Eq. (6) is

$$X = \frac{d^2}{2k\hbar\omega}, \quad (\text{B8})$$

where ω_n is the frequency of the n th radial mode. Substituting from Eq. (B2) the normalized shift is given by

$$X = \frac{0.97^2(D_e - D_h)^2}{\pi R^3 C_{11} \hbar \omega}. \quad (\text{B9})$$

The values of the parameters in Eq. (B9), for CdSe are: $D_e - D_h = 3 \text{ eV}^{17}$; $C_{11} = 7.11 \times 10^{11} \text{ dyn cm}^{-2}$.¹² For $R = 22 \text{ \AA}$, the vibrational frequency is 27 cm^{-1} . The normalized shift is 0.17 for the $n = 1$ mode.

¹For reviews, see L. E. Brus, J. Phys. Chem. **90**, 2555 (1986); IEEE J. Quantum Electron. **QE-22**, 1909 (1986); Nouveau J. Chim. **11**, 123 (1987).

- ²S. Schmitt-Rink, D. A. B. Miller, and D. S. Chemla, Phys. Rev. B **35**, 8113 (1987); E. Hanamura, Solid State Commun. **62**, 465 (1987); T. Takagahara, Phys. Rev. B **36**, 9293 (1987).
³Al. L. Efros and A. L. Efros, Fiz. Tekh. Plouprovodn. **16**, 1209 (1982) [Sov. Phys. Semiconduct. **16**, 772 (1982)].
⁴Y. Kanayama, Solid State Commun. **59**, 405 (1986); S. V. Nair, S. Sinha, and K. C. Rustagi, Phys. Rev. B **35**, 4098 (1987).
⁵M. L. Steigerwald *et al.*, J. Am. Chem. Soc. **110**, 3046 (1988).
⁶A. P. Alivisatos, T. D. Harris, P. J. Carroll, and L. E. Brus (to be published).
⁷A. M. Thayer, M. L. Steigerwald, T. M. Duncan, and D. C. Douglass, Phys. Rev. Lett. **60**, 2673 (1988).
⁸N. Chestnoy, T. D. Harris, R. Hull, and L. E. Brus, J. Phys. Chem. **90**, 3393 (1986).
⁹N. M. Dimitrijevic and P. V. Kamat, J. Phys. Chem. **91**, 2096 (1987), and references therein.
¹⁰Typical values for II-VI bulk free exciton linewidths are on the order of 0.1 meV, and are even narrower for bound excitons. See M. Dagenais and W. F. Sharfin, J. Opt. Soc. Am. B **2**, 1179 (1985).
¹¹The relevant exciton-phonon coupling mechanisms in the bulk are discussed by R. Loudon, Proc. R. Soc. London Ser. A **275**, 218 (1963); A. Pinczuk and E. Burstein, in *Light Scattering in Solids*, edited by M. Cardona (Springer, Berlin, 1983); B. K. Ridley, *Quantum Processes in Semiconductors* (Clarendon, Oxford, 1982).
¹²*Landolt-Bornstein Numerical Data and Functional Relationships in Science and Technology*, edited by K. H. Hellwege (Springer, Berlin, 1982), New Series, Vol. 17b.
¹³J. Friedrich and D. Haarer, Angew. Chem. Int. Ed. Engl. **23**, 113 (1984); B. Dick and B. Nickel, Chem. Phys. Lett. **110**, 131 (1986).
¹⁴K. F. Freed, Top. Appl. Phys. **15**, 23 (1976).
¹⁵C. Kittel, *Quantum Theory of Solids* (Wiley, New York, 1963), Chap. 7; J. Bardeen and W. Shockley, Phys. Rev. **80**, 72 (1950); A. I. Anselm and I. A. Firsov, Sov. Phys. JETP **1**, 139 (1955).
¹⁶A. E. H. Love, *A Treatise on the Mathematical Theory of Elasticity*, 4th ed. (Cambridge University, Cambridge, 1927), Chap. 12.
¹⁷A. Blacha, H. Presting, and M. Cardona, Phys. Status Solidi B **126**, 11 (1984).